The Use of Partial Cloudiness in a Warm-Rain Parameterization: A Subgrid-Scale Precipitation Scheme

PETER BECHTOLD, JEAN PIERRE PINTY, AND PATRICK MASCART

Laboratoire d'Aérologie, Université Paul Sabatier, Toulouse, France

(Manuscript received 22 September 1992, in final form 24 May 1993)

ABSTRACT

A method is proposed on how to handle the effects of partial cloudiness in a warm-rain microphysical scheme and how to generate subgrid-scale precipitation. The method is simple and concerns essentially two ideas: the use of the vertical distribution of the partial cloudiness and the use of environmental and cloud-scale values for the thermodynamic variables instead of their grid-mean values. It applies to any microphysical scheme.

Here, the method has been applied to a warm-rain parameterization scheme that has been implemented in a mesoscale model using a statistical partial cloudiness scheme. Numerical tests have been done for two one-dimensional cases of boundary-layer cloudiness: a cumulus case and a case of a decoupled stratocumulus layer.

The results show that the correct coupling of a partial cloudiness scheme and a microphysical scheme allows for a better description of the actual cloudiness and precipitation fields by ensuring a consistent computation of partial cloudiness, cloud water, and rainwater in partly cloudy regions.

1. Introduction

In addition to prognostic equations for the thermodynamic variables entropy or temperature, and total water content or specific humidity, recent mesoscale numerical weather prediction models (Sundqvist et al. 1989; Ballard et al. 1991; Pudykiewicz et al. 1992) and general circulation models (Smith 1990; Le Treut and Li 1991; Smith and Randall 1992) now use one or more prognostic equations for cloud water species (cloud water, cloud ice, rainwater) together with a diagnostic partial cloudiness scheme and a convection scheme. In the models of Sundqvist et al. (1989), Pudykiewicz et al. (1992), Ballard et al. (1991), and Smith (1990), precipitation—a sink for the cloud water content—is simply computed from an empirical formula describing the transformation of cloud water into rainwater. In these models, the effects of partial cloudiness on the precipitation rates have been introduced by using the cloud-scale water content q_c/N, with N the partial cloudiness, instead of the corresponding grid-scale value q_c. In the most recent model of Smith and Randall (1992), precipitation is calculated using a bulk microphysical parameterization, where the evaporation term is expressed as a function of the cloud-scale and environmental values of the temperature and the specific humidity, instead of using the corresponding grid-mean values. The cloud-scale and environmental variables are computed from the knowledge of the grid-scale partial cloudiness.

A common characteristic of the aforementioned models is that the partial cloudiness and the cloud water content are computed independently. Another approach is possible when a statistical partial cloudiness scheme is used (Mellor 1977), as it can diagnose both the partial cloudiness and the cloud water content. This approach is generally adopted in models that explicitly resolve deep convection. For example, the small-scale convection model of Redelsperger and Sommeria (1986) or the detailed model of the stratocumulus-capped boundary layer of Chen and Cotton (1987) calculate precipitation rates with a prognostic equation for the rainwater content using a warm-rain parameterization of the Kessler type (Kessler 1969). These models possess detailed turbulence schemes allowing for accurate calculations of turbulence production by buoyancy effects (condensation, liquid water loading), and they even try to account for the influence of precipitation on the turbulent structure. However, only Chen and Cotton (1987) attempted to include in a more general way the effects of subgrid-scale variability in a rain parameterization by adding to the microphysical production terms of autoconversion and accretion the corresponding subgrid-scale correlation term. However, this approach depends only on the turbulence level in the cloud and ignores information on the partial cloudiness, that is, the horizontal distribution of the microphysical variables, which are defined only in a fraction (cloudy or clear sky) of the numerical grid. Furthermore, the authors did not explicitly account for the evaporation of rainwater in partly satu-

Corresponding author address: Dr. Peter Bechtold, Laboratoire d'Aérologie, Université Paul Sabatier, 118, Route de Narbonne, 31062 Toulouse Cedex, France.

rated layers. When this effect is neglected, a model will always produce evaporation in partly (nonsaturated) cloudy layers.

The major point of this paper is to address the question of how to include explicitly the effects of partial cloudiness into a microphysical scheme and to generate subgrid-scale precipitation. The modified microphysical scheme should be sufficiently versatile for application to subgrid-scale convective and subgrid-scale stratiform cloudiness and precipitation. Here, we propose to handle the effects of partial cloudiness in a warm-rain parameterization in a simple way, using only the parameter partial cloudiness. It will be shown that a realistic description of the microphysical processes of evaporation, autoconversion, and accretion in partly cloudy layers must account for the vertical distribution of the partial cloudiness. Furthermore, the microphysical processes must be calculated using cloud-scale and environmental values of the thermodynamical variables instead of using their corresponding grid-mean values.

Although these general ideas are valid for any microphysical scheme, they have been applied here to the Berry and Reinhardt warm-rain parameterization (Berry and Reinhardt 1974). By predicting both the mixing ratios and number concentrations, the Berry and Reinhardt (BR) scheme is more general and allows, as was shown by Richard and Chaumerliac (1989), for a more accurate description of cloud microphysics than does the Kessler parameterization. Indeed, the developments presented in this paper can also be easily extended to the Kessler parameterization or to any other microphysical parameterization scheme.

In the next section we first briefly describe the way in which the Berry and Reinhardt (BR) rain parameterization has been coupled with the partial cloudiness scheme, and the thermodynamical framework used in the mesoscale model described in Bechtold et al. (1992, hereafter referred to as B92). We then derive the essential modifications to the BR scheme that allow for the representation of subgrid-scale precipitation. Finally, one-dimensional numerical tests are done with realistic vertical distributions of partial cloudiness inside the marine boundary layer in order to demonstrate the effects of partial cloudiness on the simulated precipitation rates in comparison with the original microphysical scheme.

2. Basic equations

Thermodynamics are described by prognostic equations for the quasi-conservative variables liquid potential temperature θ_l and total water content q_w, defined by

$$\theta_l = \theta\left(1 - \frac{Lq_l}{C_pT}\right) \tag{1}$$

$$q_w = q_v + q_l, \quad \text{where} \quad q_l = q_c + q_r. \tag{2}$$

A list of symbols is provided in the Appendix. As a convention of notation, all variables used denote grid averages at model level k. Only if necessary, superscripts k, $k+1$, etc., will be used. The cloud water content q_c is diagnosed with the aid of a statistical partial cloudiness scheme using the saturation measure $\Delta = q_w - q_s(T_l) - q_r$ with $T_l = \theta_l(T/\theta)$, instead of $\Delta = q_w - q_s(T_l)$ in the original scheme (Mellor 1977), which does not consider precipitation. The cloud-droplet concentration is a given model parameter and is assumed constant in space and time. However, the rainwater content q_r and its number concentration n_r are calculated in the BR parameterization from prognostic equations. The complete set of conservation equations for the liquid potential temperature, the total water content, the rainwater mixing ratio, and the total number concentration is

$$\frac{d\theta_l}{dt} = -\frac{L\theta}{C_pT}\frac{\partial q_r}{\partial t}\bigg|_{\text{prec}} + \frac{\partial \theta_l}{\partial t}\bigg|_{\text{rad}} + F_{\theta_l} \tag{3a}$$

$$\frac{dq_w}{dt} = \frac{\partial q_r}{\partial t}\bigg|_{\text{prec}} + F_{q_w} \tag{3b}$$

$$\frac{dq_r}{dt} = \frac{\partial q_r}{\partial t}\bigg|_{\text{auto}} + \frac{\partial q_r}{\partial t}\bigg|_{\text{accr}} + \frac{\partial q_r}{\partial t}\bigg|_{\text{eva}} + \frac{\partial q_r}{\partial t}\bigg|_{\text{prec}} \tag{3c}$$

$$\frac{dn_r}{dt} = \frac{\partial n_r}{\partial t}\bigg|_{\text{auto}} + \frac{\partial n_r}{\partial t}\bigg|_{\text{self}} + \frac{\partial n_r}{\partial t}\bigg|_{\text{eva}} + \frac{\partial n_r}{\partial t}\bigg|_{\text{prec}}, \tag{3d}$$

where the operator d/dt stands for the total derivative in an Eulerian coordinate system and where F denotes vertical turbulent diffusion. For simplicity, no vertical diffusion is applied to (3c) and (3d), as the turbulent fluxes of rainwater-related (nonconservative) variables require a complex treatment (Redelsperger and Sommeria 1982). The radiation term has been retained in (3a). Store is laid here on the form of the microphysical production terms in (3c) and (3d) as they are the terms for autoconversion, accretion, self-collection, evaporation, and precipitation. In the case of partly cloudy layers these terms apply only to the clear or cloudy parts of the numerical grid, in contrast to q_r and n_r, which are average values over the cloudy and clear-sky fraction of the grid.

3. Partial cloudiness in microphysics

Some of the production terms in (3c) and (3d) can be calculated using the cloud-scale water content q_c/N, where q_c and N are the grid-mean cloud water mixing ratio and the partial cloudiness as obtained from the partial cloudiness scheme. Then, these terms are scaled (multiplied by N) in order to obtain grid-mean values of q_r and n_r. However, some problems arise due to the fact that cloud water (cloudiness) and rainwater are independent variables. Therefore, when partly cloudy layers are present we do not know if raindrops

are falling into the clear-sky or cloudy fraction of the grid. This problem becomes apparent when we have to calculate the collection of cloud droplets by raindrops (accretion term) or the evaporation of rain in partly cloudy layers. In the following we will discuss the form of each production term in (3c) and (3d) when a BR-type parameterization is used together with a partial cloudiness scheme. All microphysical coefficients and constants appearing in the following discussion are explained in Berry and Reinhardt (1974), Nickerson et al. (1986), and Richard and Chaumerliac (1989).

a. Autoconversion

The conversion rate of cloud water into rainwater is given by

$$\left.\frac{\partial q_r}{\partial t}\right|_{\text{auto}} = \alpha \rho q_c^2 \tag{4a}$$

$$\left.\frac{\partial n_r}{\partial t}\right|_{\text{auto}} = c_\alpha \rho \left.\frac{\partial q_r}{\partial t}\right|_{\text{auto}}, \tag{4b}$$

where ρ is the air density, α a coefficient depending on the cloud-drop number concentration, and c_α a constant. The effects of partial cloudiness N can be simply taken into account by setting

$$\left.\frac{\partial q_r}{\partial t}\right|_{\text{auto}} = \alpha \rho \left(\frac{q_c}{N}\right)^2 N = \alpha \rho q_c^2 F_{\text{auto}}; \quad F_{\text{auto}} = \frac{1}{N} \tag{5a}$$

$$\left.\frac{\partial n_r}{\partial t}\right|_{\text{auto}} = c_\alpha \rho \left.\frac{\partial q_r}{\partial t}\right|_{\text{auto}}. \tag{5b}$$

The additional autoconversion factor F_{auto} was obtained in (5a) by using the cloud-scale value q_c/N and remultiplication by N, as autoconversion occurs in the cloudy part of the grid. Because equation (4a) is nonlinear, different results are obtained when we calculate the autoconversion term using grid-mean values (4a) or when we calculate local production and then take the grid mean (5a).

b. Accretion

The collection of cloud droplets by raindrops due to differences in the terminal velocity is given by

$$\left.\frac{\partial q_r}{\partial t}\right|_{\text{accr}} = \frac{3\rho}{2\rho_l D_{rm}} b_a(D_{rm}, D_c) q_r q_c, \tag{6}$$

where ρ_l is the density of liquid water and b_a is the collision efficiency coefficient as defined in Nickerson et al. (1987); D_{rm} and D_c are the diameters corresponding to the predominant mass of the rainwater spectrum and to the mean diameter of the cloud droplets, respectively. These parameters are invariant when either grid-mean or local values of q_r and n_r are used, because they are functions of the ratios q_r/n_r and q_c/n_c, respectively.

The problem of introducing the effects of partial cloudiness in (6) is more difficult than in (5) because we encounter a product of two independent variables, q_r and q_c. While cloud water is concentrated in a fraction N of the grid volume, rainwater can occur in both the cloudy and clear-sky fraction of the grid volume. To determine the accretion rate in the presence of partly cloudy layers, we have to estimate the grid fraction occupied by the rainwater and determine the horizontal overlap between the cloudy and rainwater fractions of the grid volume. In the present approach we consider only the two model layers k and $k+1$ (k is increasing with height).

In fact, we have to distinguish between two cases. First, when q_r^{k+1}, the rainwater content in the layer $k+1$ just above the considered model layer k is zero, rainwater issues in layer k, and the layer fraction occupied by the rainwater is identical to N. Consequently, (6) can be written according to (5a). However, when q_r^{k+1} is nonzero, that is, when rain from layer $k+1$ falls into layer k, we do not know a priori the grid fraction occupied by the rainwater. Starting at the top of the model (layer k_{top}), the grid fraction Cov_r occupied by q_r^{k+1} can be estimated by the cloud cover between the top of the model and layer $k+1$. The vertically integrated cloud cover in a grid column is calculated with the aid of the formula given by Sundqvist et al. (1989):

$$\text{Cov}_r = 1 - \prod_{l=k_{\text{top}}}^{k-1} \frac{1 - \max(N^{l-1}, N^l)}{1 - N^l}, \tag{7}$$

where the individual cloudy layers in the grid column overlap randomly when N varies nonmonotonically with height but overlap following the maximum overlap assumption when N varies monotonically with height. These assumptions are consistent with the statistical analysis of Tian and Curry (1989). Clearly, this formulation overestimates the rain cover when nonprecipitating cloud layers (e.g., high clouds) are present above the considered model layer k. To avoid this problem, Cov_r is set to zero when the rainwater content in layer $k+1$ is zero.

We now have to evaluate the portion of the rainwater that reacts with the cloud water. Three different vertical

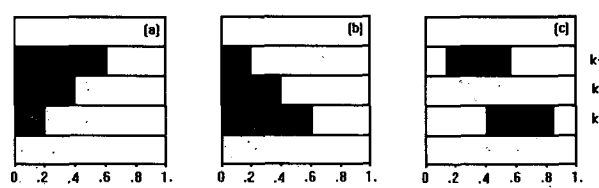

FIG. 1. Vertical distributions of the partial cloudiness: (a) monotonically increasing with height, (b) monotonically decreasing, and (c) statistical overlap.

distributions of partial cloudiness (Fig. 1) have to be considered. In the first two scenarios the cloud fraction increases/decreases monotonically with height (Figs. 1a,b), whereas in the third scenario, the cloud layers separated by a clear-sky layer overlap statistically. Three model layers with corresponding partial cloudiness, N^k, N^{k+1}, and N^{k+2}, are depicted in each figure, and we wish to calculate the accretion rate in layer k with the aid of an additional accretion factor in (6). The rain cover, evaluated at level $k+1$ with the aid of (7), is equal to N^{k+2} in Figs. 1a,c, and equals N^{k+1} in Fig. 1b. It is illustrated in Fig. 2 by the hatched areas together with the overlap region between Cov_r and N^k (shaded areas). The amount of rain from layer $k+1$ that can accrete cloud water in layer k is proportional to the overlap between Cov_r and N^k. Denoting these overlap areas by λ, and replacing q_r and q_c by their local values, we can easily derive the grid-mean accretion rates for each scenario (a)–(c) of Fig. 2:

$$\frac{\lambda}{\mathrm{Cov}_r}\frac{q_r}{\mathrm{Cov}_r}\frac{q_c}{N}\lambda = q_r q_c \frac{N}{\mathrm{Cov}_r^2}; \quad \lambda = N \tag{8a}$$

$$\frac{q_r}{\mathrm{Cov}_r}\frac{q_c}{N}\lambda = q_r q_c \frac{1}{N}; \quad \lambda = \mathrm{Cov}_r \tag{8b}$$

$$\frac{\lambda}{\mathrm{Cov}_r}\frac{q_r}{\mathrm{Cov}_r}\frac{q_c}{N}\lambda = q_r q_c N; \quad \lambda = N\,\mathrm{Cov}_r. \tag{8c}$$

The leading factor λ/Cov_r on the left-hand side of (8) gives the portion of the rainwater (scaled by its fractional cover) that can react with the cloud water; the final factor λ is necessary in order to obtain grid-mean reaction (accretion) rates. In (8a) and (8b), λ has been calculated from the maximum overlap assumption, whereas the random overlap assumption has been used in (8c). Note also that q_r is the rainwater content at level k and not at level $k+1$. The choice of $\lambda = \mathrm{Cov}_r$ instead of $\lambda = N$ in (8b) is somewhat arbitrary but ensures the right expression in the limiting cases $\mathrm{Cov}_r \to 0$ and $\mathrm{Cov}_r = N$. We can now rewrite (6) with the accretion factors derived in (8):

$$\left.\frac{\partial q_r}{\partial t}\right|_{\mathrm{accr}} = \frac{3\rho}{2\rho_l D_{rm}} b_a(D_{rm}, D_c) q_r q_c F_{\mathrm{accr}} \tag{9}$$

$$q_r^{k+1} = 0, \quad F_{\mathrm{accr}} = 1/N$$

$$q_r^{k+1} > 0, \quad F_{\mathrm{accr}} = \begin{cases} N/\mathrm{Cov}_r^2; & N^{k+1} > N^k \\ 1/N; & N^{k+1} \leqslant N^k \\ N; & N^{k+1} = 0. \end{cases}$$

An interesting feature of (9) is that the so calculated accretion rate is lower ($F_{\mathrm{accr}} < 1$) than in the original equation (6) if $q_r^{k+1} > 0$ and if $N < \mathrm{Cov}_r^{1/2}$ or $N^{k+1} = 0$. A result that is contradictory to that given in Chen and Cotton (1987), who proposed an unconditionally enhanced accretion rate due to subgrid-scale correlations between q_r and q_c. The difference is explained by the fact that (9) takes into account the possibility that rain falls into the clear-sky fraction of the grid, and so cannot interact with the cloud water.

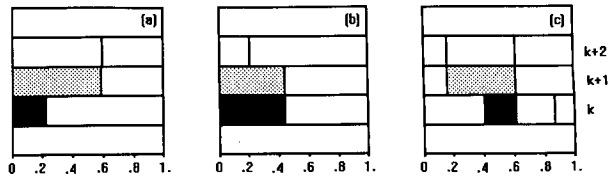

FIG. 2. Scheme corresponding to Fig. 1, which determines the amount of rainwater (covering the shaded fraction of layer $k+1$) that falls into the cloudy part of layer k. The overlap region is marked by the dark area.

c. *Self-collection*

Self-collection describes the process by which collision between raindrops produces larger drops. It is expressed as

$$\left.\frac{\partial n_r}{\partial t}\right|_{\mathrm{self}} = -\rho b_s(D_{rm}, D_r) n_r q_r, \tag{10}$$

where b_s is a collection coefficient. The product of two rainwater-related variables occurs in (10), but the problem remains similar to the accretion case, where we had to specify the reaction rate between one rainwater- and one cloud-water-related variable. In fact, (10) can be written in the same way as (9) if we assume that significant self-collection rates can occur only when larger raindrops issuing near cloud top encounter smaller ones on their path through the cloud:

$$\left.\frac{\partial n_r}{\partial t}\right|_{\mathrm{self}} = -\rho b_s(D_{rm}, D_r) n_r q_r F_{\mathrm{self}}, \tag{11}$$

with the self-collection factor defined as the accretion factor in (9).

d. *Precipitation*

The precipitation rate corresponds to the vertical gradient of the raindrops sedimentation flux. It is written as

$$\left.\frac{\partial q_r}{\partial t}\right|_{\mathrm{prec}} = \frac{\partial}{\partial z}\left[\frac{n_r m^0 v^0}{\rho} f_1(\sigma_0, D_0)\right] \tag{12a}$$

$$\left.\frac{\partial n_r}{\partial t}\right|_{\mathrm{prec}} = \frac{\partial}{\partial z}\left[n_r v^0 f_2(\sigma_0, D_0)\right], \tag{12b}$$

where v^0 and m^0 are the fall speed and the mass of a drop of diameter D_0, and where f_1 and f_2 are functions depending on the distribution parameters σ_0 and D_0 (Nickerson et al. 1987). By its definition (flux per unit surface), the formulation of the grid-mean precipita-

tion rate remains unchanged when a partial cloudiness scheme is used.

e. Evaporation

The evaporation rate of rainwater is given by

$$\left.\frac{\partial q_r}{\partial t}\right|_{\text{eva}} = \frac{\rho_l}{\rho} f_3(\sigma_0, D_0) A(T, P) S[q_v - q_s(T)] n_r, \tag{13a}$$

where A is a thermodynamical function of pressure and temperature, and S the undersaturation. All raindrops having a diameter smaller than D_{crit} evaporate during one model time step Δt. Their number is calculated by

$$\left.\frac{\partial n_r}{\partial t}\right|_{\text{eva}} = \int_0^{D_{\text{crit}}} N(D) dD, \tag{13b}$$

with

$$\int_{D_{\text{crit}}}^{0} DdD = \int_t^{t+\Delta t} A(T, P) S[q_v - q_s(T)] dt.$$

To calculate the evaporation of rain in partly saturated layers, we must know the temperature and the humidity in the clear-sky fraction of the grid. To do so, we write the grid-mean temperature and the grid-mean specific humidity as a sum of their clear-sky or unsaturated (superscript u) and cloudy or saturated (superscript s) fractions, respectively:

$$T = NT^s + (1 - N)T^u \tag{14a}$$

$$q_v = Nq_v^s + (1 - N)q_v^u \tag{14b}$$

$$q_v^s = q_s(T^s). \tag{14c}$$

This set of equations is not closed, because we have three equations for four unknown variables. To close this system, Xu and Randall (1992) assumed that the cloud-scale virtual temperature is equal to the environmental virtual temperature. However, when this closure is applied to (14), an iteration is necessary to compute T^s. Furthermore, the so-computed cloud-scale temperature T^s is not necessarily higher than the environmental temperature T^u. Instead, we propose to solve (14a) directly with the aid of the variable $T_l = \theta_l(T/\theta) = \theta_l(P/P_0)^{R/C_p}$ and the definition of $\theta_l = \theta[1 - (Lq_c/C_pT)]$, so that the solution of (14a) is

$$T^s = T_l + \frac{Lq_c/N}{C_p}; \quad T^u = T_l. \tag{15a}$$

This solution implies that the cloud-scale liquid potential temperature is approximately equal to the environmental liquid potential temperature; that is, $\theta_l^s = \theta_l^u[1 - O(10^{-4})]$. Equation (15a) is consistent with the method by which the grid-mean temperature $T = T_l + (Lq_c/C_p)$ is computed in the model, and it ensures that $T^s > T > T^u$, which is verified in the absence of subsidence warming due to cumulus convection. Knowing T^s, q_v^u is obtained from (14b),

$$q_v^u = \frac{q_v - Nq_s(T^s)}{1 - N}. \tag{15b}$$

Equation (13a) is linear with respect to the raindrop number concentration n_r. So we obtain the evaporation factor by dividing n_r by its fractional coverage Cov_r and by remultiplying (13a) with the cloudless fraction of layer k in which rainwater is present. This cloudless fraction is determined from Fig. 2 and is $\text{Cov}_r - \lambda$, the difference between the rain cover Cov_r and the overlap region between Cov_r and N. The evaporation factor then becomes $(\text{Cov}_r - N)/\text{Cov}_r = 1 - N/\text{Cov}_r$ for Fig. 2a, 0 for Fig. 2b, and $(\text{Cov}_r - \text{Cov}_r N)/\text{Cov}_r = 1 - N$ for Fig. 2c, so that the evaporation term writes

$$\left.\frac{\partial q_r}{\partial t}\right|_{\text{eva}} = \frac{\rho_l}{\rho} f_3(\sigma_0, D_0) A(T^u, P) S \times [q_v^u - q_s(T^u)] n_r F_{\text{eva}}, \tag{16a}$$

$$F_{\text{eva}} = \begin{cases} 1 - N/\text{Cov}_r, & N^{k+1} > N^k \\ 0, & N^{k+1} \leq N^k \\ 1 - N, & N^{k+1} = 0. \end{cases}$$

Note that (16a) differs from the original expression (13a) not only by an additional factor F_{eva} but also by the definition of the undersaturation that is now a function of $[q_v^u - q_s(T^u)]$, instead of $[q_v - q_s(T)]$ in (13a). Finally, (13b), which gives the number of raindrops that evaporate during one model time step, changes following (16a); that is, we replace $q_s(T)$ by $q_s(T^u)$, q_v by q_v^u, and introduce the factor F_{eva},

$$\left.\frac{\partial n_r}{\partial t}\right|_{\text{eva}} = \int_0^{D_{\text{crit}}} N(D) dD F_{\text{eva}}, \tag{16b}$$

with

$$\int_{D_{\text{crit}}}^{0} DdD = \int_t^{t+\Delta t} A(T^u, P) S[q_v^u - q_s(T^u)] dt.$$

f. Summary of the scheme

The modified set of equations is distinguished from the original one by the use of additional factors, taking into account the vertical distribution of the partial cloudiness, and by the use of incloud and environmental values for T and q_v in order to describe correctly the evaporation in partly cloudy layers. The only free parameter that must be determined in the scheme is Cov_r, the grid fraction occupied by rainwater. Exclusively in the case $N^{k+1} > N^k$ (Fig. 1a), this parameter intervenes in the accretion–self-collection factor by a quadratic term and in the evaporation factor by a linear

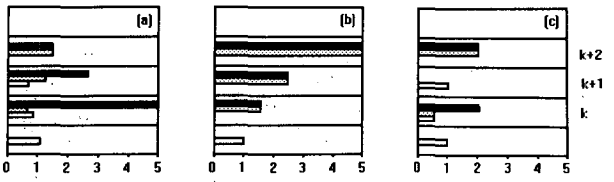

FIG. 3. Vertical distributions of the autoconversion factor (dark), the accretion factor (hatched), and the evaporation factor (open), corresponding to the cloudiness profiles in Fig. 1.

term; otherwise, the factors depend only on the parameter partial cloudiness.

The work of the modified set of equations is illustrated in Fig. 3, where we have drawn the values of the additional microphysical factors F_{auto} (shaded bars), F_{accr} (hatched bars), and F_{eva} (open bars) for the three cloudiness distributions shown in Fig. 1. Whereas the autoconversion factor is simply inversely proportional to the partial cloudiness, the accretion factor (self-collection factor) depends on the cloudiness distribution considered. It has been chosen equal to the autoconversion factor for the uppermost partly cloudy layer and for distribution (b); however, its value varies between 0 and $1/N$ for the other distributions chosen; for example, its value is close to one in layer k^*+1 of Fig. 3a, and 0.5 in layer k of Fig. 3c. Concerning the evaporation factor, we see that it is zero for the cloudiness distribution (b), but also for the uppermost partly cloudy layer of the other distributions. This is clearly different from the original formulation that would simulate evaporation because the grid-mean humidity in a partly cloudy (saturated) grid is lower than its saturation value. However, the evaporation factor is one, so it is identical to the original formulation, in the subcloud layer.

In summary, the introduction of additional factors allows for a versatile handling of the effects of partial cloudiness in a bulk microphysical scheme. Whereas an additional autoconversion factor has already been considered by Redelsperger and Sommeria (1986), Chen and Cotton (1987), and Sundqvist et al. (1989), the authors did not consider the effects of partial cloudiness on the rain evaporation rate. We show in Fig. 3 that these effects cannot be neglected. However, the full advantages of the modified set of equations, especially of the modified evaporation equation (16), which uses the temperature and humidity in the cloudless part of the grid, can be documented only for realistic cases of subgrid-scale cloudiness and precipitation.

4. Numerical tests

Two documented cases of partial cloudiness in the marine boundary layer have been chosen for the numerical tests. The first case is a cumulus-topped boundary layer observed during FIRE [First ISCCP (International Satellite Cloud Climatology Project) Regional Experiment] by Betts and Boers (1990); the second one is a case of North Atlantic stratocumulus clouds observed by Nicholls and Leighton (1986). The chosen cases provide typical profiles of partial cloudiness and have already been modeled by B92, including cloud radiation and cloud turbulence interaction but without microphysical processes. However, when partial cloudiness is simulated with the aid of a statistical partial cloudiness scheme, the corresponding cloud water content is in general rather low. As a consequence, the simulated rainwater content and, especially, the microphysical terms of accretion and self-collection are rather small. Nevertheless, our principal interest in the following numerical tests is to realistically demonstrate the differences in the evaporation rates calculated with the original BR rain parameterization and the modified scheme.

The one-dimensional tests have been run for one hour with a vertical resolution of 50 m and a time step of 10 s, during which the microphysical equations (3c) and (3d) are integrated with a Runge–Kutta scheme of order 4. The model top is set to 3 km. For both cases, the cloud droplet number concentration is set to 50 cm^{-3}, a typical value for marine boundary layer clouds. Furthermore, the solar radiation conditions are fixed to 1200 LST. All initial thermodynamical and turbulent profiles are balanced and issue from the corresponding simulations described in B92.

a. Cumulus case

The corresponding initial vertical profiles of the partial cloudiness and the cloud water content are depicted in Fig. 4. The cloudiness profile is close to the schematic profile depicted in Fig. 1a. It shows a cloud layer of 300-m thickness and maximum partial cloudiness of

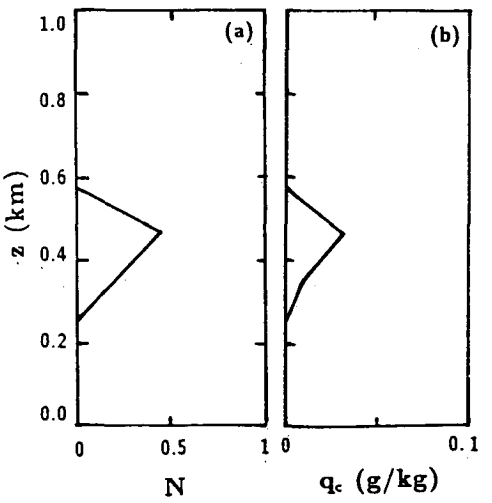

FIG. 4. Initial distributions of the partial cloudiness (a) and the cloud water content (b) for the cumulus case.

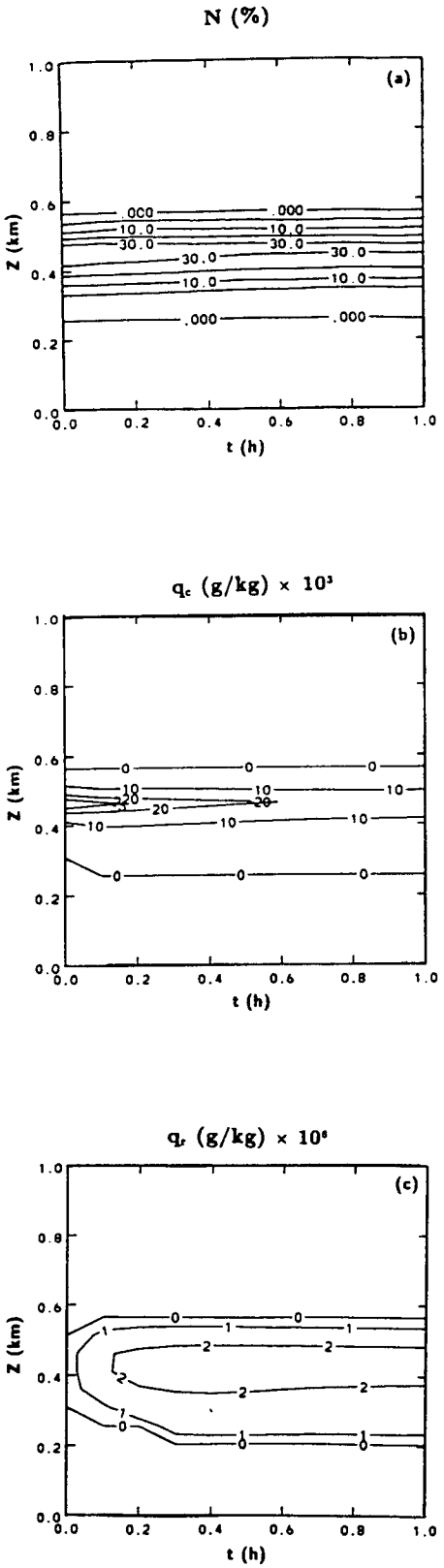

FIG. 5. One-hour evolution of (a) the partial cloudiness, (b) the cloud water content, and (c) the rainwater content.

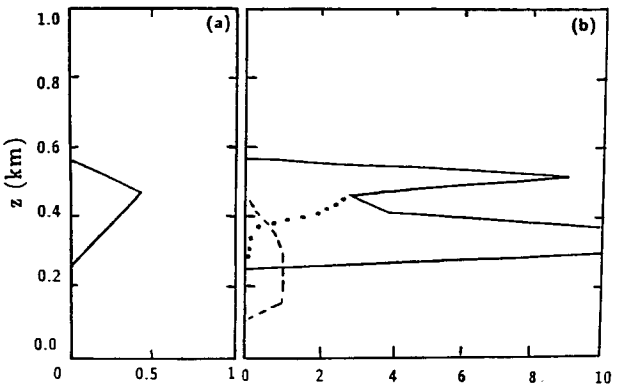

FIG. 6. Profile of the partial cloudiness after 1080 s, together with the corresponding profiles for the additional microphysical factors for autoconversion (solid line), accretion (dotted line), and evaporation (dashed line).

37%. The maximum cloud water content (not shown) is 0.025 g kg^{-1}. The simulated evolution over one hour of the partial cloudiness, the cloud water content, and the rainwater content is shown in Fig. 5. The partial cloudiness (Fig. 5a) scarcely varies during the simulation. Its maximum value reduces from 37% initially to 35% after one hour of simulation. However, the evolution of the cloud and rainwater content is very rapid. After about 10 min the cloud and rainwater content becomes stationary (Figs. 5b,c). The cloud has lost about 50% of its initial water content by precipitation. The maximum rainwater content attains a value of 3×10^{-6} g kg^{-1}, a rather small value that is a factor of 10^4 smaller than the maximum cloud water content.

The additional microphysical factors of autoconversion (F_{auto}), accretion (F_{accr}), and evaporation (F_{eva}) used in the modified BR parameterization [Eqs. (5), (9), and (16)] are shown after 18 min of simulation in Fig. 6, where the corresponding profile of the partial cloudiness is also drawn. The profiles of the microphysical factors are close to those schematically depicted in Fig. 3a. However, the autoconversion factor shows a double maximum due to the low values of cloudiness at cloud top and cloud base. Note also that the accretion factor is greater than one in the layer with maximum cloudiness. The evaporation factor continuously increases from zero to unity when one approaches the cloud base. The different evaporation rates calculated according to (13) with the original scheme (OS) and according to (16) with the modified scheme (MS) are illustrated in Fig. 7, where we have actually plotted the undersaturation multiplied by the evaporation factor (which is one in the OS). Figure 7 shows remarkable differences between the two schemes. Whereas the MS does not allow for evaporation in the upper part of the cloud (the evaporation factor is zero), the OS simulates strong undersaturation and therefore evaporation. The differences between the two schemes persist in the lower part of the cloud, where the MS

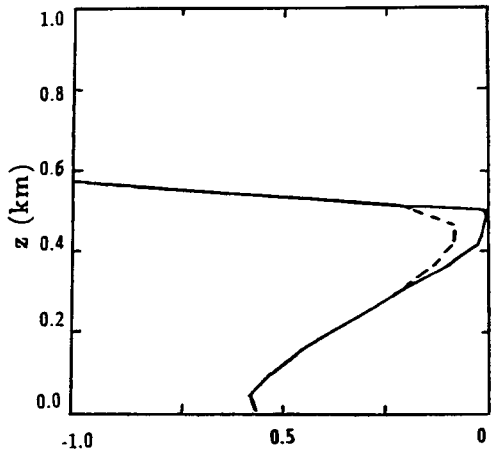

FIG. 7. Comparison of the vertical profiles of the saturation deficit multiplied by the evaporation factor, obtained with the modified scheme (solid line) and with the original scheme (dashed line).

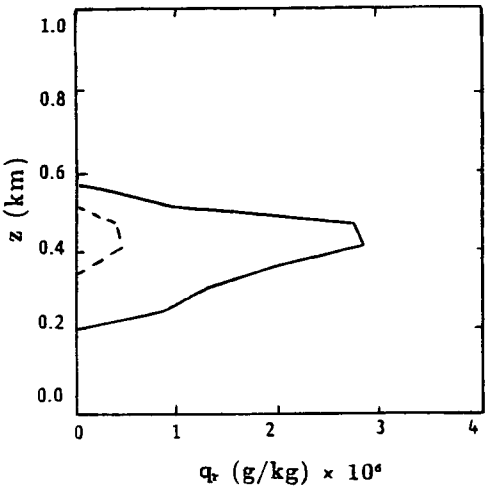

FIG. 8. Comparison of the vertical profiles of the rainwater content obtained with the modified scheme (solid line) and with the original scheme (dashed line).

smoothly approaches the OS when one approaches the cloud base. Finally, in Fig. 8 we compare the rainwater content obtained with the MS to that obtained with the OS. The results are shown after one hour of simulation. The MS produces a cloud water content that is about a factor of 6 larger than that obtained with the OS. Furthermore, in the MS scheme, rain falls down to a height of 200 m, which is two levels below cloud base, whereas in the OS the rainwater content is so small that all rain immediately evaporates below cloud base. The differences in the rainwater content between the two schemes are mainly due to the higher autoconversion rate and lower evaporation rate simulated by the MS. About 70% of the difference in Fig. 8 can be explained by the additional autoconversion factor in the MS, but 30% of the difference is due to the different formulations of evaporation used in the two schemes.

b. Stratocumulus case

This case centers on a decoupled cloud-layer structure, where a cumulus cloud layer with maximum cloudiness of 30% has formed under the main stratocumulus cloud deck (Fig. 9). The cumulus layer is decoupled from the overlying stratocumulus by a shallow, stable layer. This case is very close to that schematically depicted in Fig. 1c and is characteristic of a stratocumulus cloud deck that has been partly evaporated near its base during daytime due to the absorption of solar radiation. In Fig. 10 we show the simulated 1-h evolution of the partial cloudiness, the cloud water content, and the rainwater content. After about 40 min of simulation, the cloudless layer between 600 and 700 m has entirely disappeared (Figs. 10a,b), and the stratocumulus cloud deck has reconnected to the underlying cumulus layer. This notable evolution is due not only to the evaporation and the recondensation of rainwater in the cloudless layer between the stratocumulus cloud deck and the cumulus layer but also to thermodynamical instability in the subcloud layer caused by the surface heat and moisture fluxes. As a consequence of this instability, the stable layer that separated the cumulus layer from the stratocumulus layer disappears, and the precipitating stratocumulus cloud (Fig. 10c) can be supplied with humidity from below. Note that the cloud water content in Fig. 10b does not decrease in spite of losses by precipitation, because it is fed by the surface moisture flux. However, a detailed discussion of this thermodynamical instability and the diurnal variations of stratocumulus clouds due to precipitation and radiation processes is out of the scope of this paper, and we refer the interested reader to Paluch and Lenschow (1991).

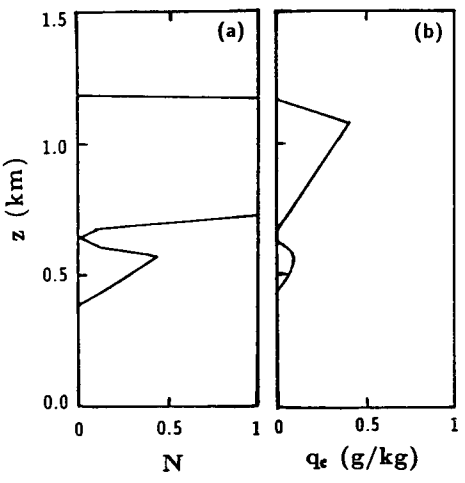

FIG. 9. As in Fig. 4 but for the decoupled stratocumulus case.

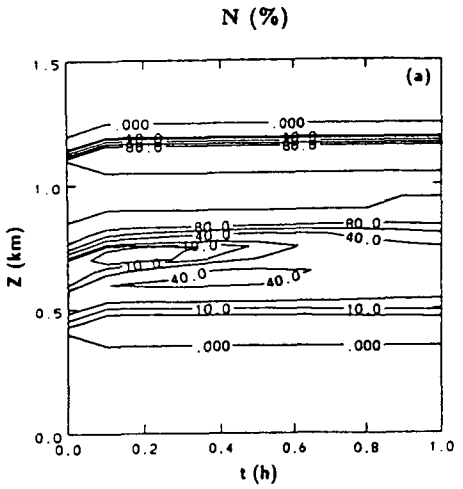

FIG. 10. Same as Fig. 5.

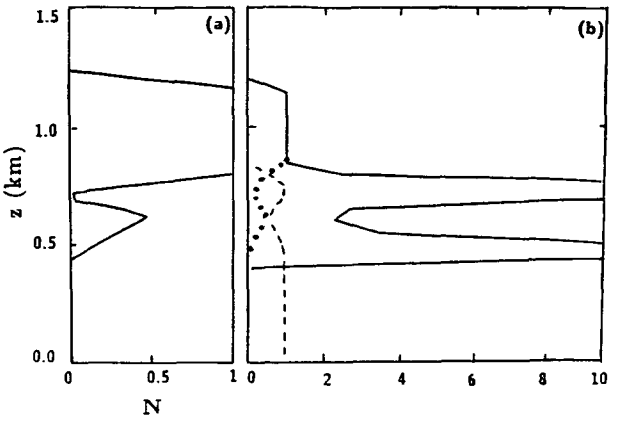

FIG. 11. Same as Fig. 6.

As in Fig. 6b, we have depicted in Fig. 11b the additional factors for autoconversion, accretion, and evaporation of the MS, corresponding to the partial cloudiness profile after 18 min of simulation (Fig. 6a). Evidently, one retrieves the double structure of the partial cloudiness in the microphysical factors; maximum values for the autoconversion and evaporation factor correspond to minimum values for the accretion factor, and vice versa. When the partial cloudiness reaches 100% in the stratocumulus layer, the values for the accretion and evaporation factors inside the cumulus layer are simply given by N and $1 - N$, respectively. In Fig. 12 we have compared the undersaturation as calculated by the OS with the undersaturation multiplied by the evaporation factor as calculated by the MS. The OS simulates evaporation even in the stratocumulus layer where the cloudiness is 100%. This is an artifact of the statistical partial cloudiness, where the partial cloudiness and the grid-mean temperature and humidity are derived from a linearized form of the saturation equation. As a consequence, the

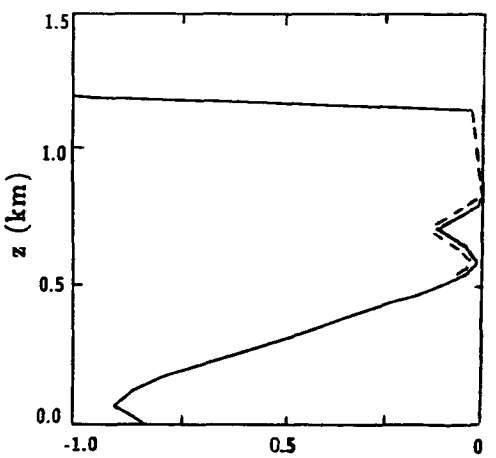

FIG. 12. Same as Fig. 7.

grid-mean humidity slightly differs from its saturation value, especially in regions of high cloud water content. This deficiency of the OS has been naturally remedied in the MS, which simulates saturation due to an evaporation factor of zero. In general, the MS produces stronger undersaturation than the OS because of the use of environmental instead of grid-mean values for the temperature and the humidity. But this tendency is counterbalanced by the evaporation factor, so that the net result in Fig. 12 is slightly smaller evaporation in the MS than in the OS.

A comparison of the rainwater content obtained after one hour of simulation with either of the two schemes is shown in Fig. 13. The maximum rainwater content obtained with the MS is 11.5×10^{-3} g kg^{-1} compared to 10.4×10^{-3} g kg^{-1} with the OS. However, whereas the relative difference in the rainwater content between the two schemes is about 9% near cloud top, it attains 20% at the surface. The higher rainwater content produced by the MS in comparison to the OS is mainly due to the fact that the MS simulates less evaporation (Fig. 12). The influence of the additional autoconversion factor is minor in this case because rainwater is mainly produced near the top of the stratocumulus where the cloudiness is 100%. This is confirmed by Fig. 14, where we have displayed the main production and sink terms in the budget of q_r [Eq. (3c)], as they are the terms of autoconversion, precipitation, and evaporation. The terms of accretion and self-collection are negligible in the present case. In the upper part of the stratocumulus layer the autoconversion term is balanced by the precipitation term, whereas the latter term is balanced by the evaporation term in the cumulus layer and the subcloud layer.

5. Summary and conclusions

A method has been proposed to include the effects of partial cloudiness in a microphysical scheme and to generate subgrid-scale precipitation. The proposed method essentially profits by two ideas: the use of the vertical profile of the partial cloudiness, and the use of cloud-scale and environmental values of the thermodynamic variables instead of their grid-mean values. As an example, these general ideas have been applied to a Berry and Reinhardt warm-rain parameterization scheme.

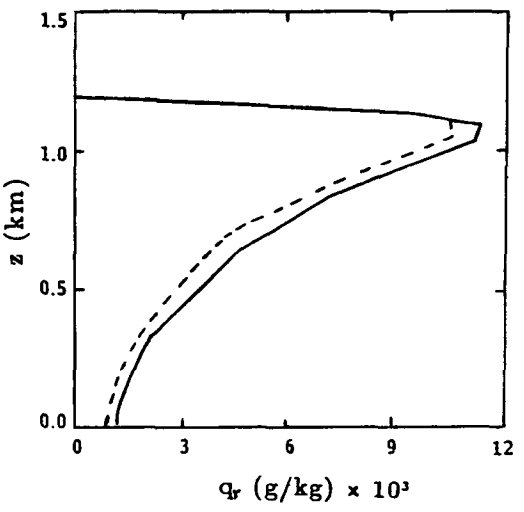

FIG. 13. Same as Fig. 8.

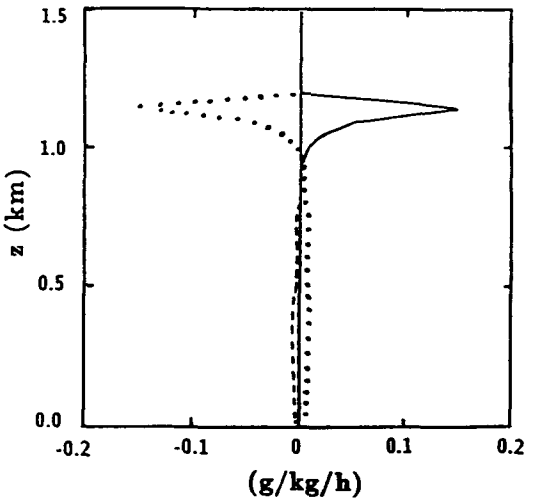

FIG. 14. Rainwater budget. Solid line: autoconversion rate; dotted line: sedimentation rate; dashed line: evaporation.

The necessary modifications to the original Berry and Reinhardt scheme are simple and concern mainly the introduction of additional factors for autoconversion, accretion, self-collection, and evaporation. These factors are calculated as functions of the vertical profile of the partial cloudiness only. Another important difference to the original scheme concerns the calculation of the saturation deficit, where estimates of the temperature and humidity in the cloudless part of the grid are used instead of the corresponding grid-mean values.

The modified scheme has been compared to the original scheme for two typical cases of boundary-layer cloudiness. The first case corresponds to a cumulus cloud layer with maximum partial cloudiness of 37%, while the second one is a typical stratocumulus cloud deck with an underlying cumulus layer. In these numerical experiments the precipitation rates are rather low. The rainwater budget is determined by the rates of autoconversion and evaporation; the production of rain by accretion or self-collection was negligible. It has been shown that the modified BR parameterization produces larger precipitation rates (subgrid-scale precipitation) than the original scheme. Furthermore, the effects of partial cloudiness must also be considered in the evaporation term and cannot be neglected compared to the effects on the autoconversion term, as it was done in earlier work. This point is particularly important in regions with low values of the partial cloudiness, where the grid is strongly undersaturated.

The present scheme ensures a consistent computation of partial cloudiness, cloud water, and rainwater, and proposes a first step in developing methods for an explicit computation of precipitation amounts in partly cloudy regions. However, work has still to be done in order to test the scheme in the case of deeper convective cloudiness with higher cloud water and rainwater amounts and to test when the accretion and self-collection terms become important.

Acknowledgments. We wish to thank Prof. R. Rosset and Drs. E. Richard and K. Suhre for their helpful comments and suggestions. Special thanks go to Mrs. J. Duron, who developed the graphic software. This work was supported by grants from Institut National des Sciences de l'Univers (ATP PAMOS). Computer resources have been made available by C.C.V.R. (Palaiseau, France).

APPENDIX

List of Principal Symbols

b_a, b_s Collision efficiency coefficients
c_α Autoconversion constant
C_p Heat capacity
Cov_r Grid fraction occupied by the rainwater
D_c Mean cloud-droplet diameter
D_r Mean raindrop diameter
D_{rm} Raindrop diameter for the predominant mass
D_{crit} Critical diameter
D_0 Distribution parameter for the lognormal distribution
L Latent heat of evaporation
m^0 Mass of a raindrop of diameter D_0
N Partial cloudiness
n_c Cloud-droplet concentration
n_r Raindrop concentration
P_0 Reference pressure (1000 hPa)
q_c Specific cloud water content
q_l Specific liquid water content
q_r Specific rainwater content
q_s Saturation specific humidity
q_v Specific humidity
q_w Specific total water content
R Gas constant for dry air
t Time
T Temperature
v^0 Terminal fall speed of a raindrop of diameter D_0
z Vertical coordinate
α Autoconversion coefficient
θ Potential temperature
θ_l Liquid potential temperature
ρ Density of air
ρ_l Density of liquid water
σ_0 Dispersion parameter for the lognormal distribution

REFERENCES

Ballard, S. P., B. Golding, and R. N. B. Smith, 1991: Mesoscale model experimental forecasts of the haar of northeast Scotland. *Mon. Wea. Rev.*, **119,** 2107–2123.

Bechtold, P., C. Fravalo, and J. P. Pinty, 1992: A model of marine boundary-layer cloudiness for mesoscale applications. *J. Atmos. Sci.*, **49,** 1723–1744.

Berry, E. X., and R. L. Reinhardt, 1974: An analysis of cloud drop growth by collection. Part III: Accretion and self-collection. *J. Atmos. Sci.*, **31,** 2118–2126.

Betts, A. K., and R. Boers, 1990: A cloudiness transition in a marine boundary layer. *J. Atmos. Sci.*, **47,** 1480–1496.

Chen, C., and W. R. Cotton, 1987: The physics of the marine stratocumulus-capped mixed layer. *J. Atmos. Sci.*, **44,** 2951–2977.

Kessler, E., 1969: *On the Distribution and Continuity of Water Substance in Atmospheric Circulation, Meteor. Monogr.*, No. 32, Amer. Meteor. Soc., 84 pp.

Le Treut, H., and Z.-X. Li, 1991: Sensitivity of an atmospheric general circulation model to prescribed SST changes: Feedback effects associated with the simulation of cloud optical properties. *Climate Dyn.*, **5,** 175–187.

Mellor, G. L., 1977: The Gaussian cloud model relations. *J. Atmos. Sci.*, **34,** 356–358.

Nicholls, S., and J. Leighton, 1986: An observational study of the structure of stratiform cloud sheets. Part I: Structure. *Quart. J. Roy. Meteor. Soc.*, **112,** 431–460.

Nickerson, E. C., E. Richard, R. Rosset, and D. R. Smith, 1986: The numerical simulation of clouds, rain, and airflow over the Vosges and Black Forest mountains: A meso-β model with parameterized microphysics. *Mon. Wea. Rev.*, **114,** 398–414.

Paluch, I. R., and D. H. Lenschow, 1991: Stratiform cloud formation in the marine boundary layer. *J. Atmos. Sci.*, **48,** 2141–2158.

Pudykiewicz, R., R. Benoît, and J. Mailhot, 1992: Inclusion and verification of a predictive cloud-water scheme in a regional numerical weather prediction model. *Mon. Wea. Rev.*, **120,** 612–626.

Redelsperger, J. L., and G. Sommeria, 1982: Méthode de représentation de la turbulence associée aux précipitations dans un modèle tri-dimensionnel de convection nuageuse. *Bound.-Layer Meteor.*, **24,** 231–252.

——, and ——, 1986: Three-dimensional simulation of a convective storm: Sensitivity studies on subgrid parameterization and spatial resolution. *J. Atmos. Sci.*, **43,** 2619–2635.

Richard, E., and N. Chaumerliac, 1989: Effects of different rain parameterizations on the simulation of mesoscale orographic precipitation. *J. Appl. Meteor.*, **28,** 1197–1212.

Smith, L. D., and D. A. Randall, 1992: Parameterization of cloud microphysics processes in the CSU General Circulation Model. Atmospheric Science Paper No. 491, Colorado State University.

Smith, R. N., 1990: A scheme for predicting layer clouds and their water content in a general circulation model. *Quart. J. Roy. Meteor. Soc.*, **116,** 435–460.

Sundqvist, H., E. Berge, and J. E. Kristjánsson, 1989: Condensation and cloud parameterization studies with a mesoscale numerical weather prediction model. *Mon. Wea. Rev.*, **117,** 1641–1657.

Tian, L., and J. A. Curry, 1989: Cloud overlap statistics. *J. Geophys. Res.*, **94,** 9925–9935.

Xu, K.-M., and D. A. Randall, 1992: The semi-empirical basis of a prognostic cloud parameterization for use in climate models. *Proc. 11th Int. Conf. on Clouds and Precipitation,* Montreal, Canada, 1144–1147.